

See discussions, stats, and author profiles for this publication at: <https://www.researchgate.net/publication/373350805>

Experimental and modeling analysis of the transient spray characteristics of cyclopentane at sub- and transcritical conditions using a machine learning approach

Article in Physics of Fluids · August 2023

DOI: 10.1063/5.0159979

CITATIONS

7

4 authors:



Thangaraja Jeyaseelan

Vellore Institute of Technology University

60 PUBLICATIONS 1,213 CITATIONS

[SEE PROFILE](#)

READS

368



Min Son

University of the Bundeswehr Munich

82 PUBLICATIONS 503 CITATIONS

[SEE PROFILE](#)



Tobias Sander

University of the Bundeswehr Munich

67 PUBLICATIONS 205 CITATIONS

[SEE PROFILE](#)



Lars Zigan

University of the Bundeswehr Munich

147 PUBLICATIONS 2,237 CITATIONS

[SEE PROFILE](#)

RESEARCH ARTICLE | AUGUST 23 2023

Experimental and modeling analysis of the transient spray characteristics of cyclopentane at sub- and transcritical conditions using a machine learning approach

Thangaraja Jeyaseelan   ; Min Son  ; Tobias Sander   ; Lars Zigan 



Physics of Fluids 35, 083119 (2023)

<https://doi.org/10.1063/5.0159979>



View
Online



Export
Citation

CrossMark

Articles You May Be Interested In

Large eddy simulations of a transcritical round jet submitted to transverse acoustic modulation

Physics of Fluids (May 2016)

Transcritical transition of the fluid around the interface

Physics of Fluids (December 2021)

The Infra-Red and Raman Spectra of Cyclopentane, Cyclopentane- d_1 , and Cyclopentane- d_{10}

J. Chem. Phys. (December 2004)

Experimental and modeling analysis of the transient spray characteristics of cyclopentane at sub- and transcritical conditions using a machine learning approach

Cite as: Phys. Fluids **35**, 083119 (2023); doi: [10.1063/5.0159979](https://doi.org/10.1063/5.0159979)

Submitted: 29 May 2023 · Accepted: 8 August 2023 ·

Published Online: 23 August 2023



View Online



Export Citation



CrossMark

Thangaraja Jeyaseelan,^{1,a)} Min Son,² Tobias Sander,^{2,a)} and Lars Zigan^{2,3}

AFFILIATIONS

¹Automotive Research Centre, School of Mechanical Engineering, Vellore Institute of Technology, Vellore 632 014, India

²Institut für Thermodynamik, Professur für Energiewandlung, Fakultät für Luft- und Raumfahrttechnik, Universität der Bundeswehr München (UniBwM), D-85577 Neubiberg, Germany

³Erlangen Graduate School in Advanced Optical Technologies (SAOT), Friedrich-Alexander-Universität Erlangen-Nürnberg (FAU), D-91052 Erlangen, Germany

^{a)}Authors to whom correspondence should be addressed: thangaraja.j@vit.ac.in and Tobias.Sander@unibw.de

ABSTRACT

Although fuel spray parameters, such as spray cone angle and penetration length, are crucial for developing high-efficiency and high-performance combustion engines, general models for predicting transient characteristics of these parameters have not been suggested. In this study, the spray characteristics of cyclopentane at sub- and transcritical conditions relevant for IC engine and rocket injections were experimentally evaluated. A single simplified model for predicting the spray cone angles and spray penetration lengths over time was developed by adopting artificial neural networks (ANN). Spray measurements were conducted by shadowgraphy and Mie scattering techniques to recognize the phase change behavior of the spray, changing the injection and chamber conditions. The ANN model was developed using a multi-layer network with six normalized inputs and four outputs. It was trained with five transient spray datasets at two subcritical and three transcritical injection conditions. It was validated with one transcritical spray dataset. The ANN prediction was assessed, and the proposed approach represents the spray characteristics of cyclopentane at sub- and transcritical conditions. According to the model results, the predicted spray parameters are in good agreement with the experimental results over a useful pressure and temperature range of 40–55 bar and 465–564 K, mean absolute percentage errors of 2.25% (shadowgraphy) and 4.92% (Mie) for the spray angles, and 1.11% (shadowgraphy) and 3.44% (Mie) for the spray penetration lengths. Moreover, the developed ANN model can predict the penetration ratio, providing information on phase changes in sprays. The developed ANN model in this study is expected to become a universal model for transient spray characteristics near the critical point. By adding the database with various fuel types and spray conditions, the universal model can be used to develop high-efficiency and high-performance combustion engines or other combustors.

Published under an exclusive license by AIP Publishing. <https://doi.org/10.1063/5.0159979>

I. INTRODUCTION

The fuel spray evolution, including the breakup and phase change processes, is crucial as it governs subsequent processes such as mixing, ignition, combustion, and pollutant formation. A comprehensive assessment of the spray characteristics of fossil and biofuels with advanced injection systems provide valuable insight into the in-chamber processes. The characteristics of fuel sprays especially the alternative fuels, such as alcohols,^{1,2} biodiesels,^{3,4} and biodiesel-alcohol blends,^{5,6} were experimentally investigated following optical diagnostic

techniques by numerous researchers. Typically, the spray behavior is characterized following Mie scattering, shadowgraphy, and Schlieren photography.⁷ The major spray jet characteristics include cone angle, penetration length, and droplet diameter, such as Sauter mean diameter (SMD).^{8,9}

Researchers have modeled these parameters under varying chamber conditions¹⁰ and fuel characteristics.¹¹ Especially, machine learning (ML) technologies have gained popularity in the fuel sprays research community due to their ability to model complex physical

and chemical processes.¹² One popular ML technique is the artificial neural network (ANN). The ANN imitates the neurological mechanisms of the human brain and has evolved from a simple architecture to a multi-layer neural network.¹³

Taghavifar *et al.*¹⁴ predicted diesel spray characteristics using ANN with a backpropagation algorithm. Input variables were normalized, and data were divided into training, validation, and testing sets. The Levenberg–Marquardt algorithm yielded the least error in their network. In contrast, Hwang *et al.*¹⁵ used machine-learning to predict the 3D liquid dispersion of various fuel sprays, using experimental data from a constant-flow spray vessel. They reported a maximum error in the liquid penetration length of 7.3% and claimed that machine learning had advantages over computational fluid dynamics for similar spray parameters. Hwang *et al.*¹⁶ further combined CFD and ANN models to predict and compare spray dynamics of single-component and multi-component fuels. To avoid issues like underfitting and over-fitting, they advocated for a properly constructed neural network with the best arrangement found for two hidden layers.

Regarding spray diagnostics, Wensing *et al.*¹⁷ experimented with single component and mixed fuels to study fuel phase behavior under supercritical conditions. Mie scattering and laser-induced fluorescence (LIF) spray measurements were used to capture fuel distribution, with LIF detecting both liquid and supercritical phases. A liquid to supercritical fluid transition without drastic density change was observed, though more research is needed for accurate mixture formation quantification. Lind *et al.*¹⁸ conducted planar laser-induced fluorescence (PLIF) measurements with a tracer in a transcritical diesel spray using gas-to-liquids (GTL) fuel, finding an average maximum temperature difference of about 150 K between fuel jet and ambience.

Fu *et al.*¹⁹ examined the macroscopic spray characteristics of fossil and biofuel blends using the Schlieren method and empirical models. Spray parameters, such as penetration length, cone angle, projected area, and spray droplet size, were analyzed. They concluded that model predictions were most consistent with the measurements.^{20–22} Liu *et al.*²³ proposed a feed-forward backpropagation neural network with five inputs to predict spray tip penetration lengths of different fuels, with the optimal network structure reported for 16 hidden layer neurons.

Spray characteristics are essential for designing injectors and combustion devices, but these characteristics are affected by multiple parameters and vary with time.²⁴ An optimal design point is required due to the structural and systemic restrictions of combustion engines. Therefore, a machine learning model can be a solution to predict these complicated spray characteristics. Though previous researchers have suggested models to predict spray characteristics, as discussed, the models have been restricted to predicting a couple of parameters at certain steady conditions. A universal model to predict various transient spray characteristics at various chamber conditions is a missing gap in the design of next-generation combustion engines.

The current paper primarily aims to study the spray characteristics of cyclopentane, a representative hydrocarbon fuel, with a focus on understanding and quantitatively predicting behavior under sub- and transcritical conditions. These transcritical conditions exhibit a different mixing behavior than sub-critical injections and require further consideration, for example, the phase separation processes are not yet fully understood.²⁵ In this context, transcritical injection refers to conditions where the pressure is supercritical and the temperature of

the fuel or mixture increases from subcritical to supercritical during the spray process.²⁶ Subsequently, a simple ANN modeling approach is suggested to predict spray angles, spray penetrations, and phase change characteristics over time.

II. METHODOLOGY

A. Experimental methods

The spray experiments were conducted at the Prüfzentrum in Nürnberg (PZN) operated by the Professur für Fluidsystemtechnik (FST), Friedrich-Alexander-Universität Erlangen-Nürnberg (FAU), using a high pressure high temperature injection chamber (“OptiVeP”). The chamber has the capability to operate at temperatures up to 1000 K and pressures ranging from 30 kPa to 10 MPa.²⁷ The chamber has a continuous gas flow at constant pressure and temperature fields, providing constant ambient conditions. The cubic chamber has five large quartz windows on each side and an injector flange at the bottom. A single-hole gasoline direct injection (GDI) research injector with a single injection hole of ~0.2 mm diameter was installed at the bottom flange as shown in Fig. 1.

The injector introduces the surrogate fuel in an upward direction. The fuel was pressurized by a dual-syringe pump, and the fuel temperature was controlled by heating the injector tip with a thermostat. High-speed optical diagnostics were mainly conducted using two different optical measurement methods, as shown in Fig. 1: shadowgraphy (which is actually an unfocused Schlieren setup without a schlieren knife, and the signals include light extinction due to the liquid phase of the fuel) and Mie scattering measurement. The shadowgraphy technique is used to capture the second derivatives of the ray that is distorted by different diffractive indices. These are induced by the differences in densities, temperatures, and species of media. In this experiment, the diffractive indices changed due to the differences between the ambient medium and the injected fuel and the difference between the ambient and fuel temperatures. The shadowgraphy technique can capture the whole spray regardless of the phase of the spray. The Mie scattering technique is an elastic scattering process that occurs when the ray's wavelength is much smaller than the particle size. Mie scattering is evidence of the existence of droplets. If data from both methods are combined, it is possible to identify the vaporization or phase transition region.^{7,8,17}

For the shadowgraphy method, a green LED illuminator (HARDsoft IL-105G) was used to expand the light beam, which was directed toward the high-speed camera (Photron Fastcam SA-Z). Three diffused LED lights were installed on the top window and the other two side windows for the Mie scattering measurement. To keep the same field of view, a single high-speed camera was used, and consecutive Mie scattering and shadowgraphy methods were conducted. Consequently, the two types of light sources were turned on and off alternately. Both methods were applied with a frame rate of 40 000 fps, and the shadowgraphy had an exposure time of 1 μ s, while the Mie scattering measurement had an exposure time of 5 μ s.

Researchers in previous studies have used Mie scattering and shadowgraphy techniques to obtain spray penetration lengths, which contain valuable information. However, the results from each method were analyzed separately.^{18,28,29} In this study, the penetration ratio (PR) is newly defined based on the spray penetration lengths obtained from both Mie scattering and shadowgraphy techniques, as shown in Eq. (1), where l_{Mie} and l_{shadow} denote the spray penetration lengths measured by Mie scattering and shadowgraphy techniques, respectively,

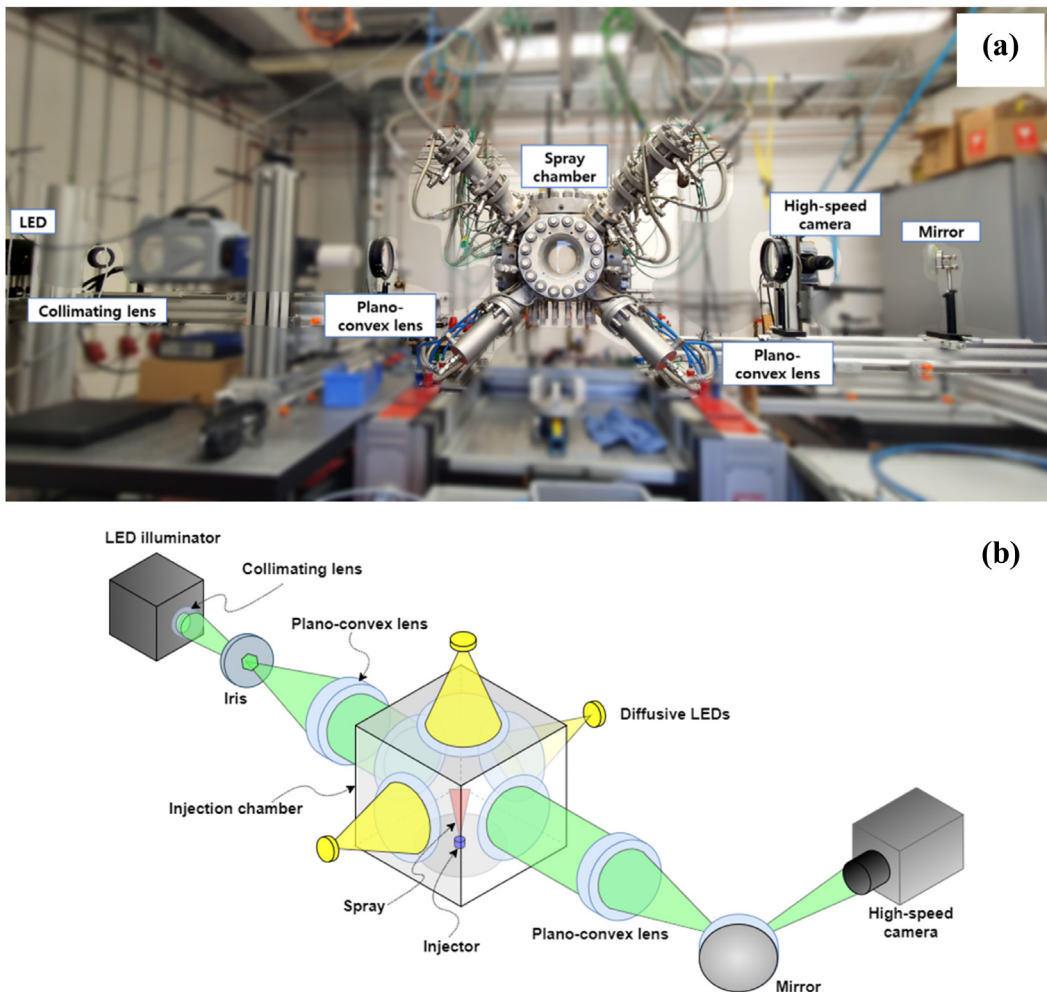


FIG. 1. Experimental setup for optical spray diagnostics: (a) a photograph of the test bench and (b) a schematic of the setup.

$$PR = \frac{l_{Mie}}{l_{shadow}}. \quad (1)$$

In other words, PR represents the ratio of the liquid spray penetration length to the total spray penetration length. A smaller PR indicates a higher evaporation rate of the liquid phase in the spray, and a broader vapor (or supercritical) phase region, which can mix with the ambient gas. Hence, a smaller PR can lead to a shorter ignition delay and an improvement in combustion efficiency.

B. Experimental conditions

Experiments were conducted at near-critical conditions, based on the fuel properties. In this research, cyclopentane was used as a surrogate fuel, and the critical points of cyclopentane and the ambient gas, nitrogen (N_2), were calculated by CoolProp³⁰ as shown in Table I.

As presented in Table II and Fig. 2, the sub- and supercritical conditions for the six studied cases were represented by changing the chamber pressure (P_c), chamber temperature (T_c), and injection

temperature (T_{inj}). The injection pressure (P_{inj}) was adjusted to maintain similar injection pressure drops ($\Delta P = P_{inj} - P_c$) of the fuel leaving the injector for various chamber pressures. The reduced pressure ($P_{r,c} = P_c/P_{cr}$) and reduced temperature ($T_{r,c} = T_c/T_{cr}$) of the chamber were calculated based on the critical point of cyclopentane, which can affect the spray characteristics under subcritical/transcritical conditions. The density (ρ_{inj}) and kinematic viscosity (ν_{inj}) of the injected fuel were calculated at the chamber pressure and injection temperature by CoolProp,³⁰ assuming the properties at the exit of the injector. A total injection time of 3 ms was applied for each case, and 32 injection shots were conducted at each operating point.

TABLE I. Critical points for the fluids under investigation.

Fluids	P_{cr} (bar)	T_{cr} (K)
Cyclopentane	45.71	511.72
Nitrogen	33.95	126.19

TABLE II. Experimental conditions and the test fuel properties.

Case	P _c (bar)	T _c (K)	P _{inj} (bar)	T _{inj} (K)	P _{r,c}	T _{r,c}	ρ _{inj} ^a (kg/m ³)	ν _{inj} ^a × 10 ⁻⁷ (m ² /s)
1	40.1	465	83.0	293	0.88	0.91	749.0	4.47
2	55.1	466	97.9	293	1.20	0.91	750.4	4.51
3	40.1	564	83.5	293	0.88	1.10	749.0	4.47
4	55.0	564	98.3	293	1.20	1.10	750.4	4.51
5	40.0	564	84.4	373	0.88	1.10	666.9	2.62
6	55.0	563	99.1	373	1.20	1.10	668.9	2.65

^aProperties at P_c and T_{inj}, calculated by CoolProp.³⁰

The uncertainties of the measured mean values for 32 shots, except the fuel temperature, were lower than 0.1% of the mean values with 95% confidence intervals,³¹ while the fuel temperature had a maximum inaccuracy of 1%. The research injector, which utilizes a commercial high-pressure gasoline operating system, was evaluated using an injection rate test. The overall uncertainty of the repeatability was found to be less than 0.5%. Case 3 was specified as the target condition for spray validation by the ANN model, and the measurements were not included in the training dataset. The next section details the development of the ANN and their preferred architecture.

C. Artificial neural network

Before selecting the appropriate ANN architecture to predict the spray parameters, it is necessary to preprocess the experimental datasets for accurate and faster convergence.³² The accuracy of the model predictions depends on the datasets used for its training. Therefore, the input and output variables were normalized and range from a minimum of 0 to a maximum of 1, using the following normalization equation:

$$y_n = \frac{y_i - y_{\min}}{y_{\max} - y_{\min}}, \quad (2)$$

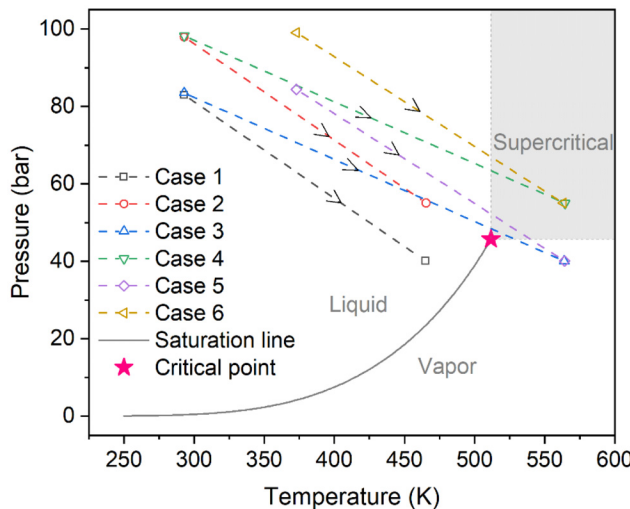


FIG. 2. Experimental conditions on a cyclopentane phase diagram.

where y_n, y_{min}, and y_{max} are the normalized, minimum, and maximum values of y_i, respectively.

The proposed ANN architecture is shown in Fig. 3, where two hidden layers with seven neurons achieved the smallest mean square error (MSE) and mean absolute percentage error (MAPE) on the test results. The neural network toolbox of MATLAB (R2019b) was used with six normalized inputs: reduced pressures, reduced temperatures, injection time, fuel density, viscosity, and four outputs/target variables, namely, the spray penetration length and spray cone angle determined by shadowgraphy and Mie scattering methods. Since the effect of surface tension cannot be assessed above the critical point as the surface tension becomes zero at supercritical conditions, it is not considered as a sensitive fuel property input in the current model. The model was trained and validated using experimental datasets. Feed-forward back-propagation was employed for training the neural network.

The training of the ANN involved the use of LM algorithm and gradient descent momentum learning function. Transfer functions were used for the hidden and output layers, including the linear and the hyperbolic tangent sigmoid transfer functions, respectively, as shown in Fig. 4. The weights (w) and biases (b) of the neurons in the adjacent layers were optimized during the adapted multilayer network training, aiming to minimize the loss function.

The model is assessed following statistical measures such as mean square error (MSE), mean absolute percentage error (MAPE), and coefficient of determination (R²), which are estimated as follows:

$$MSE = \frac{1}{n} \left\{ \sum_{i=1}^n (y_{i,\text{exp}} - y_{i,\text{ann}})^2 \right\} \quad (3)$$

$$MAPE = \frac{1}{n} \left[\sum_{i=1}^n \left| \left(\frac{y_{i,\text{exp}} - y_{i,\text{ann}}}{y_{i,\text{exp}}} \right) \right| \right] * 100 \quad (4)$$

$$R^2 = \left[1 - \frac{\sum_{i=1}^n (y_{i,\text{exp}} - y_{i,\text{ann}})^2}{\sum_{i=1}^n (y_{i,\text{ann}})^2} \right] \quad (5)$$

where y_{exp} represents the measured values obtained through experiments, and y_{ann} represents the predicted values obtained through the ANN model.

The trained ANN model with seven hidden layer neurons was established to predict the variation of spray parameters of cyclopentane at sub- and transcritical conditions. The assessment of several

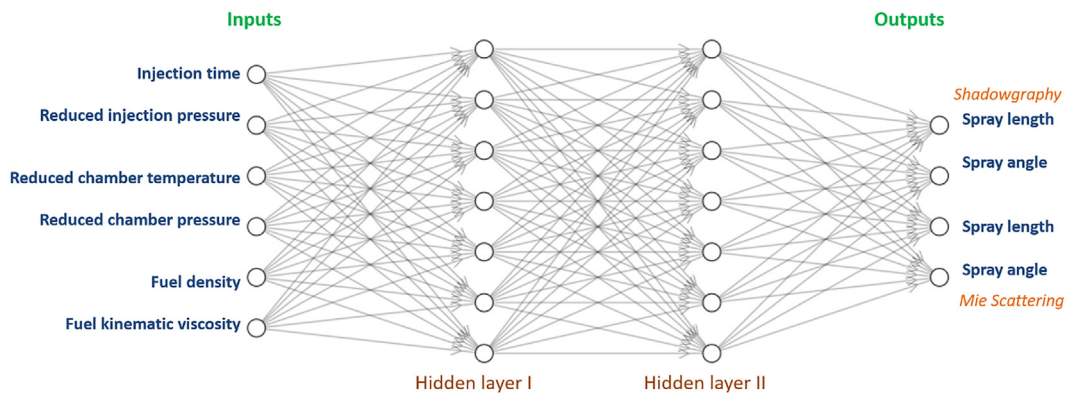


FIG. 3. ANN architecture to model the spray parameters.

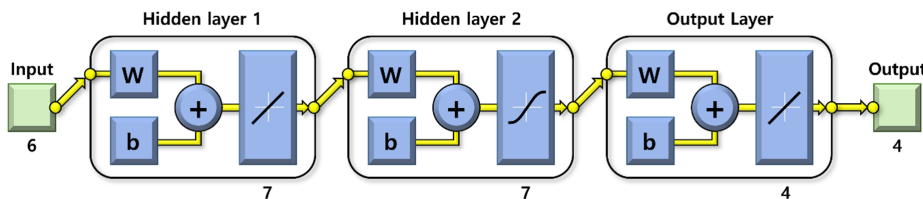


FIG. 4. Optimized multilayer network and transfer functions.

combinations of the evaluated ANN model is provided in the Appendix (Table IV), and various iterations were executed until an exact prediction of the untrained datasets was attained. The network architecture and transfer functions were modified to attain the best model results in accordance with the estimated error values.

III. RESULTS AND DISCUSSION

A. Experimental results

The spray penetration length and angle are significant parameters that provide an overview of the spray characteristics. The spray length is defined as the distance covered by the spray, and the full cone angle is the cone angle of the spray, as shown in Fig. 5. To detect the spray boundary, each spray snapshot is compared with a background image without spray. The spray boundary (red boundary in Fig. 6) is projected onto the projection plane and the line of sight of boundary pixels collected in a single row. The Radon transform of the spray boundary image is obtained by continuously rotating the spray boundary image and applying the projection.

A strong projected signal can be detected in the Radon domain when the boundary line is aligned along the projection direction. The rotated image angle is considered as the spray half angle, and two points with the strongest projection values can be obtained for each spray half angle. Since the points are picked from a location close to the zero-rotation degree, the spray angle is assumed to be measured near the injector. The spray penetration length was determined by measuring the distance between the furthest spray boundary and the injector tip from each snapshot. All measurements were performed for single images, and the ensemble averages for the spray angles and the penetration lengths were calculated from 32-shot data per case over time.

The spray angles were smoothed over time by averaging adjacent 20 points with moving windows to improve the ANN modeling, as shown in Fig. 7. The uncertainty of smoothed data at each point in time (U_t) can be calculated using Eq. (6), which combines the

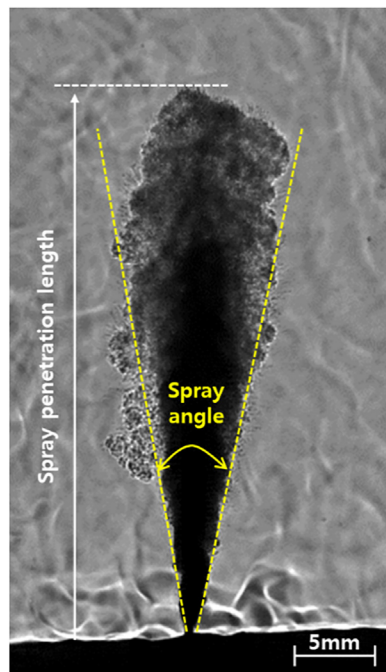


FIG. 5. Definitions of spray angle and penetration length.

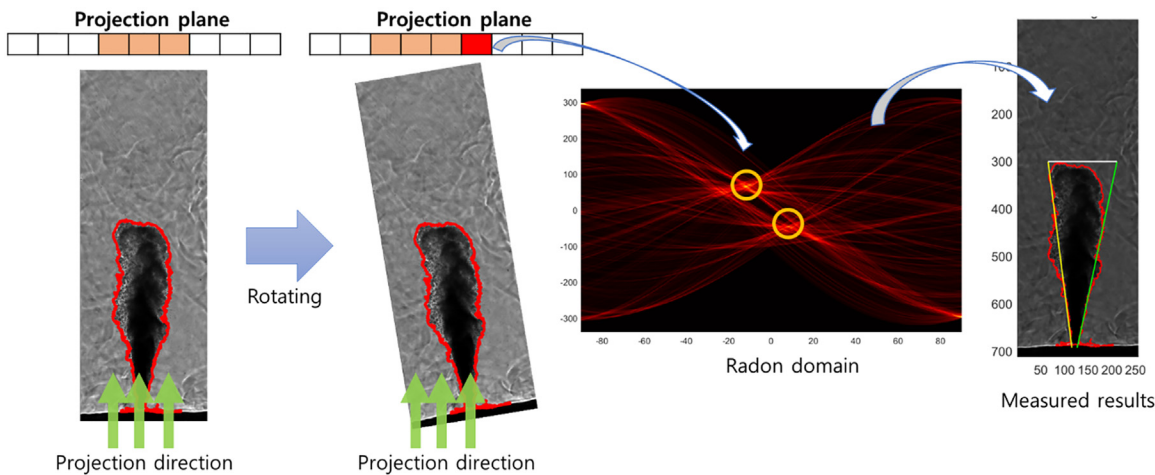


FIG. 6. Post-processing method for spray angle measurements.

uncertainty of measured point data at each moment (u_t)³¹ with the prediction interval of smoothed data (I_p)³³, as described in the following equations:

$$U_t = \sqrt{u_t^2 + I_p^2} \quad (6)$$

$$u_t = T_{n-1} \frac{\sigma(\theta_t)}{\sqrt{n}} = T_{n-1} \left[\frac{\sum_{j=1}^n (\theta_{tj} - \bar{\theta}_t)^2}{n(n-1)} \right]^{1/2} \quad (7)$$

$$I_p = T_{m-1} \sigma(\varepsilon) \sqrt{1 + \frac{1}{m}} = T_{m-1} \sqrt{(m+1) \frac{\sum_{t=1}^m (\bar{\theta}_t - X_t)^2}{m(m-1)}} \quad (8)$$

where n represents the number of shots, which is 32 in this study, and t denotes the time after start of injection. T_{n-1} represents the 97.5 percentile of Student's t-distribution with $n-1$ degrees of freedom for the 95% confidence interval, θ_t is the measured spray angle, while $\bar{\theta}_t$ is the ensemble-averaged spray angle, depicted as dots in Fig. 7. $\sigma(\theta_t)$ represents the standard deviation of the measured spray angle at each time. m is the number of times after start of injection. ε denotes the error of smoothed data, defined as the difference of the measured data and smoothed data ($\bar{\theta}_t - X_t$), and $\sigma(\varepsilon)$ is the standard deviation of this error.

The mean uncertainty (\bar{U}_t) for the smoothed spray angles derived from shadowgraphy is approximately $\pm 1.70^\circ$, and the maximum uncertainty [$\max(U_t)$] reaching approximately $\pm 3.57^\circ$. For the smoothed spray angles calculated via Mie scattering, the mean

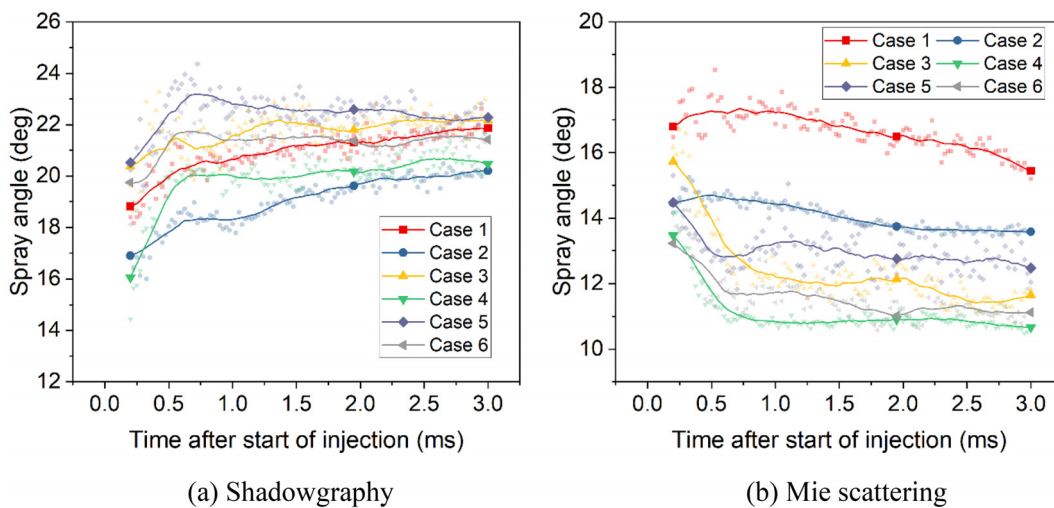


FIG. 7. Measured spray angles over time over time after start of injection.

uncertainty is approximately $\pm 1.01^\circ$, and the maximum uncertainty is around $\pm 2.46^\circ$. The spray angles from shadowgraphy for all cases show monotonic increasing trends at early injection times, and then, the spray angles converge to specific values, as shown in Fig. 7(a). On the other hand, the spray angles from Mie scattering measurements show more complicated trends. Overall, the Mie scattering spray angles are smaller than the shadowgraphy spray angles because the shadowgraphy image contains the gas-phase or supercritical fluid around the liquid spray, as shown in Fig. 7(b). The spray angles from Mie scattering show similar trends as the shadowgraphy when the chamber temperature is low (cases 1 and 2), whereas the spray angles at the higher chamber temperature converge after decreasing at early injection times, as shown in Fig. 7(b).

The spray penetration lengths from the shadowgraphy exhibit similar developing profiles in response to changes in chamber conditions, as shown in Fig. 8. With respect to spray penetration length, the uncertainty at each time after start of injection can be calculated in the same way as Eq. (7). The mean uncertainty from shadowgraphy measurements is approximately ± 0.29 mm, and the maximum uncertainty is roughly ± 0.54 mm. For the measurements obtained from Mie scattering, the mean uncertainty of the spray penetration length is about ± 0.38 mm, with the maximum uncertainty reaching approximately ± 0.74 mm. This was expected because the injector pressure was adapted to yield a similar pressure drop ΔP of about 42 bar so that the spray momentum is comparable.

On the other hand, the penetration lengths from the Mie scattering measurement showed saturation characteristics. As the sprays in cases 1 and 2 remain in the liquid phase after injection, as shown in Fig. 2, the liquid spray penetration length measured by Mie scattering follows the spray penetration length measured by shadowgraphy. The liquid jet length converges to a maximum length when the chamber temperature is high (cases 3–6), which is due to the strong evaporation caused by heat transfer from the hot gas (or transition to supercritical state, respectively), leading to shorter liquid penetration length. When comparing cases 3 and 5, both experience a phase change to vapor, as

shown in Fig. 2, but the higher injection temperature in case 5 results in a shorter liquid spray penetration length. Cases 4 and 6 display similar trends in comparison with cases 3 and 5, but the increase in chamber pressure has a limited effect on the liquid spray penetration length. Especially, the effect of injection temperature at transcritical chamber conditions (cases 5 and 6) on the liquid spray penetration length is negligible. The differences between shadowgraphy and Mie scattering images are clearly visible in Fig. 9. The spray shape captured by Mie scattering measurement is similar to the spray shape measured by shadowgraphy in case 1, whereas the Mie scattering spray images in cases 3 and 6 are narrower and shorter, indicating a more pronounced vaporization effect.

The quasi-steady characteristics of the sprays at 3 ms (Fig. 10) making the effect of injection and chamber conditions more apparent. The results at 1 and 2 ms are attached in the Appendix for completeness (Fig. 17). The spray angles determined by shadowgraphy are primarily affected by chamber pressure, while the spray angle from the Mie scattering technique is mostly influenced by chamber temperature, and both are inversely proportional to the respective control parameter, as shown in Fig. 10(a). The chamber pressure also affects the penetration length shown by the shadowgraphy, but it is less sensitive compared to the spray angle. It is also evident that an increase in the chamber temperature strongly affects the liquid spray penetration length measured by Mie scattering measurement, as shown in Fig. 10(b). On the other hand, when cases 5 and 6 are compared to cases 3 and 4, an increase in fuel injection temperature does not show any significant effects on quantitative spray characteristics compared to changes of the other experimental conditions.

Theoretically, the maximum PR has to be 1.0 because the liquid droplets exist at the end of the spray when there is no evaporation. However, the PRs at early stage were slightly over-predicted as shown in Fig. 11 because of a too small penetration length and the low image resolution. Consequently, the Mie scattering signals resulted in non-focused blurred images. Nevertheless, the trends in PR after an injection time of ~ 1.0 ms clearly highlight the differences in phase change

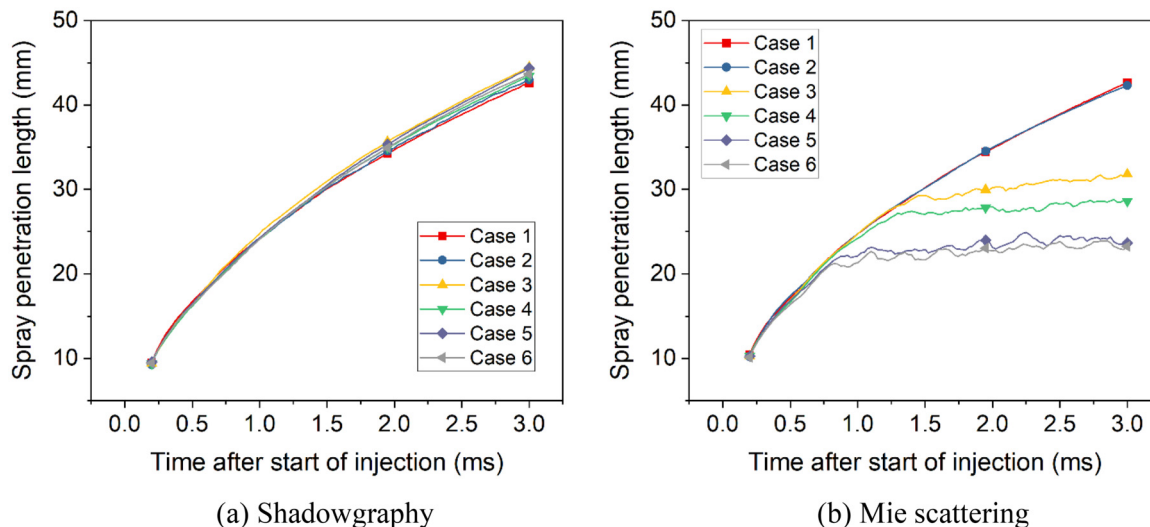


FIG. 8. Measured spray penetration lengths over time after start of injection.

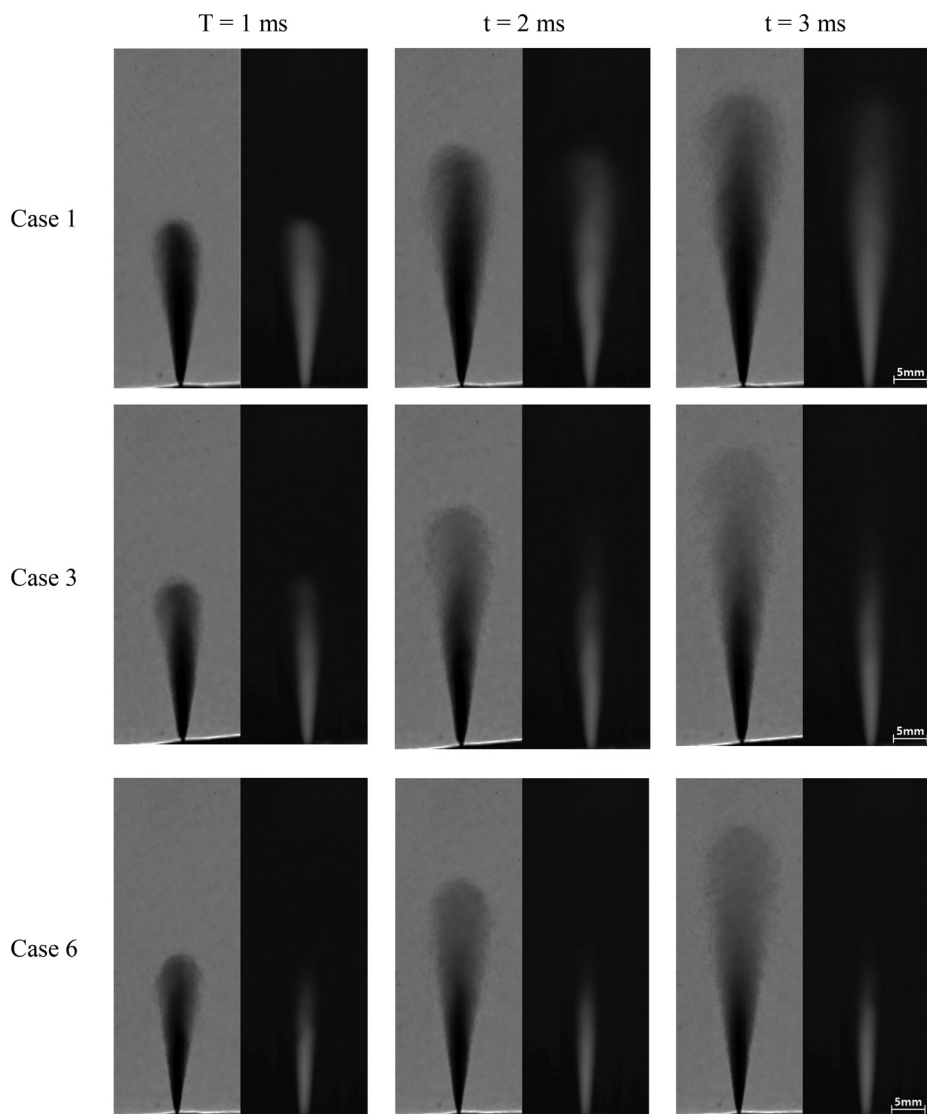


FIG. 9. Ensemble-averaged spray snapshots from shadowgraphy (left) and Mie scattering measurements (right).

characteristics of sprays at sub- and transcritical conditions. When the chamber temperature is low (cases 1 and 2), PRs remain nearly constant at 1.0, indicating that the phase change from liquid to gas occurs very slowly and the effect of chamber pressure is limited. However, when the chamber temperature is higher (cases 3 and 4), the phase change from liquid to gas or liquid to supercritical fluid occurs more rapidly, and the increase in the chamber pressure enhances this phase change. Higher injection temperatures in cases 5 and 6 further promote the phase change; in addition, the pronounced fluctuations of PR are observed. This means that the increase in injection temperature may induce cyclic variation and thus combustion instability.^{34,35}

B. Modeling and validation of the ANN model

A total of 565 measured datasets were used to develop the ANN spray model, and the best validation performance (squared mean

error) for the trained datasets was found to be 0.0004, at which point the model converged, and the training ended. Figure 12 shows the overall regression plots of the detailed data of the ANN model, which indicate a high degree of correlation. The correlation coefficients (R) were found to be 0.998 11, 0.998 16, 0.997 64, and 0.998 04 for training, validation, testing, and overall data, respectively, demonstrating the accuracy and performance of the developed ANN model and indicating that the developed ANN model has a good accuracy and performance.^{36–38} The developed ANN model is validated with untrained test results from case 3 (chamber pressure of 40.05 bar and injection pressure of 83.5 bar), and the comparative results are shown in Figs. 13 and 14 for the shadowgraphy and Mie scattering methods, respectively.

As observed, the developed ANN model can effectively predict the measured spray parameters for both methods, with mean absolute percentage errors observed as 2.25% (shadowgraphy) and 4.92% (Mie)

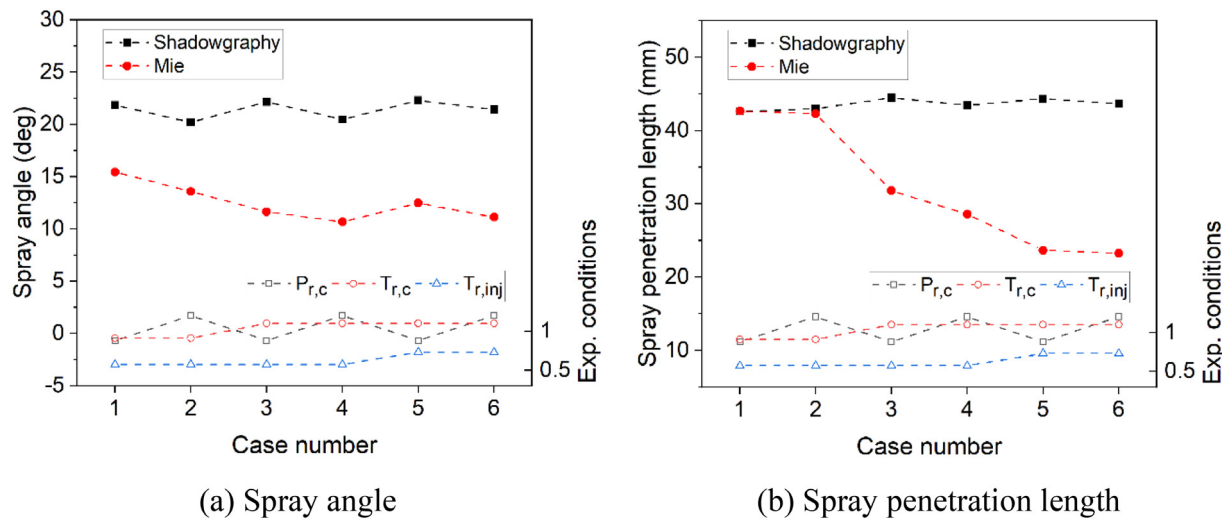


FIG. 10. Measured spray angle (left) and penetration length (right) at 3-ms injection time under various experimental conditions.

for the spray angles and 1.11% (shadowgraphy) and 3.44% (Mie) for the spray penetration lengths. Generally, the ANN model slightly underestimates the measured trends. However, it successfully models four outputs over time using a single, simple ANN structure. This is achieved within acceptable error ranges, despite the complex trends of the spray characteristics that vary depending on sub- and transcritical conditions.

Furthermore, the ANN model predictions are compared with all six measured cases, and their comparative results at the end of injection (3 ms) are shown in Fig. 15. Similar comparisons at injection times of 1 and 2 ms are provided in the Appendix for completeness (refer to Fig. 17 and Tables V and VI).

The percentage error between the ANN model and the measurements is presented in Table III. The results indicate that the developed ANN model accurately predicts the spray penetration length and spray cone angle using both shadowgraphy and Mie scattering methods at sub- and transcritical conditions. However, cases 3 and 5, which involve the most complex injection process physics, exhibit the largest deviations from the experimental data. Cases 1 and 2, which are relatively simple subcritical injections, display small deviations between the experiment and model. The same holds true for cases 4 and 6, although they involve transcritical injections.

The PR, which can be the design parameter of the combustion engine providing the phase change information, can be predicted by the developed ANN model, as shown in Fig. 16. Although the PR is not a direct output of the model, it is well predicted. The prediction accuracy decreases near the PR of 1.0, but this is due to the limitations of the original experimental data with the very short sprays as discussed in the previous section. Nevertheless, the ANN model's prediction is in good agreement with the experimental data within the 95% prediction interval,³³ as shown in Fig. 16. Further, the model could accurately predict both the static characteristics of PR for the cases 1 and 2, and the transient characteristics for the other four cases as depicted in Fig. 11; cases 1 and 2 have almost constant PR values near 1.0; therefore, PRs for both cases concentrate near 1.0 as shown in Fig. 16.

To summarize, experimental data (565 transient data points) comprising five datasets of spray parameters at various conditions are used for training the ANN model to predict the complex spray characteristics. Among the many input variables possible for the spray model, the variables having the most significant effect on the output variables have been chosen after a detailed literature survey. To accurately model the nonlinear spray characteristics, two hidden layers with seven neurons are found to be useful after several iterations. Finally, the developed model was validated with transcritical datasets (one case with 113 transient data points). The ANN prediction was

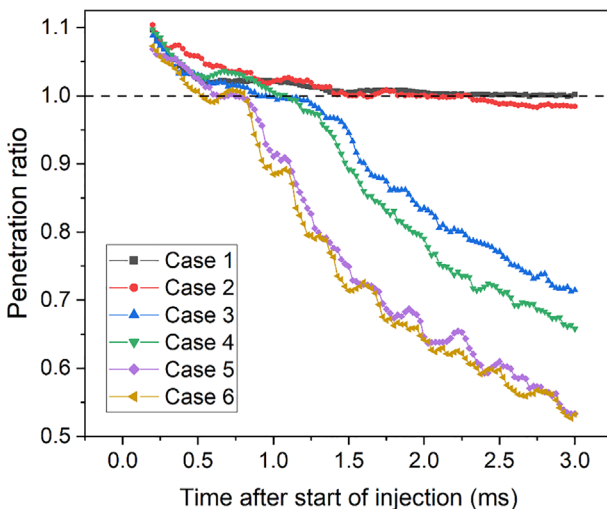


FIG. 11. Penetration ratio over time at various experimental conditions.

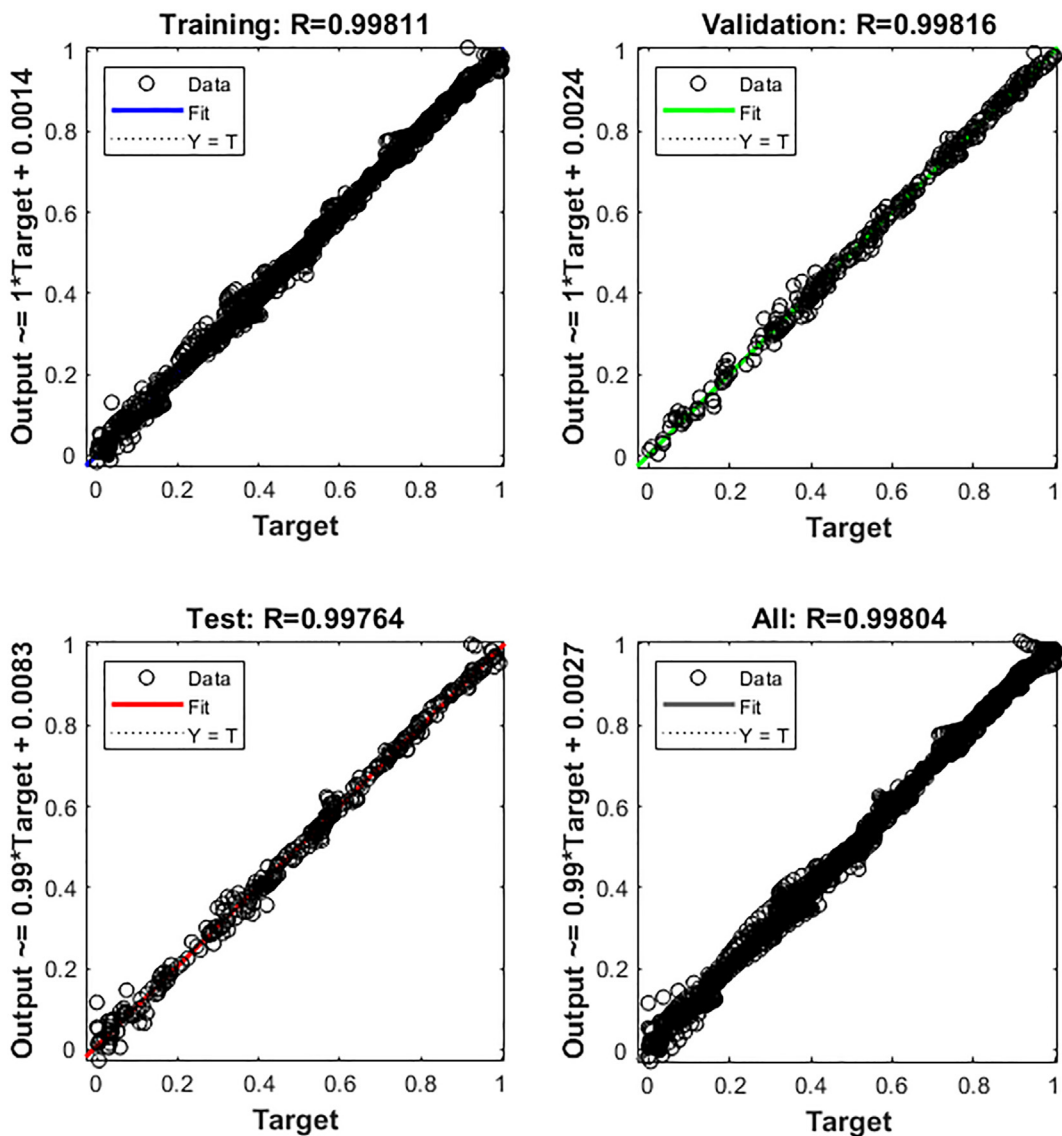


FIG. 12. Regression plots for the ANN model including training, testing, and validation.

systematically assessed, and the proposed approach represents the spray characteristics of cyclopentane at sub- and transcritical conditions. Further, the computational time of the developed ANN model is very low vis-a-vis conventional mathematical models. However, feeding any data to the ANN model, outside the trained range, will lead to a significant error. Therefore, it is essential to address this major shortcoming of ANN by developing hybrid models (integrating the physics-based model into the neural networks^{39,40}) which is considered as the future scope of the study.

IV. CONCLUSIONS

In this study, experimental studies were conducted to evaluate the spray characteristics of cyclopentane at sub- and transcritical

conditions. The spray characteristics were investigated using two optical methods based on the various chamber and injection conditions over time. The focused shadowgraphy technique was applied to capture the whole spray, including the gaseous and supercritical phase, whereas the Mie scattering signal represents the liquid phase. The spray angles and penetration lengths from both methods were analyzed at sub- and transcritical conditions. Additionally, a new parameter, the penetration ratio (PR), was introduced. PR provides phase change information, which is crucial for designing combustion engines because a faster phase change can reduce the ignition delay and improve combustion efficiency.

To model the spray characteristics (spray angles and penetration lengths controlled by injection and chamber conditions), an ANN was

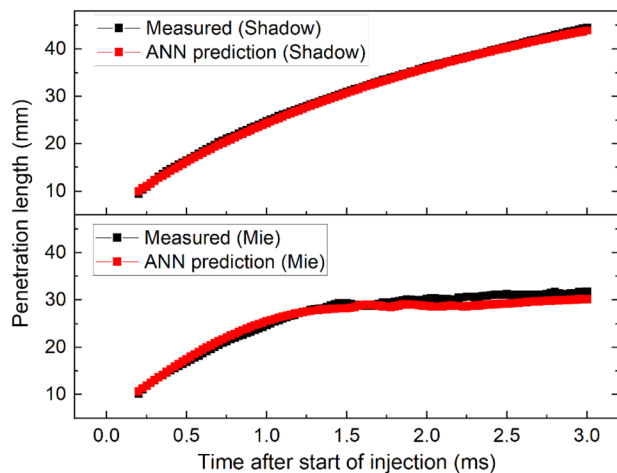


FIG. 13. Validation of spray penetration length over time (case 3).

adopted. The ANN model was trained and validated with experimental datasets, demonstrating lower MSE and MAPE values for the measured and predicted datasets. The maximum prediction error was found to be within 5% of the measured spray parameters following shadowgraphy and Mie scattering methods. Thus, the developed ANN model can estimate the critical spray parameters of cyclopentane at sub- and transcritical injection conditions. The developed ANN model is also able to effectively predict the PR even though it is not directly included as an output parameter of the model.

The results of this study can be used to design high-efficiency combustion devices, in order to predict spray targeting, e.g., spray–wall interactions and thus pollutant formation in various conditions. The proposed ANN structure can be adopted in similar applications to model spray characteristics. Based on this study, the model is expected to be expandable to a universal spray model for various fuel types (single component and multi-component fuels determining the spray

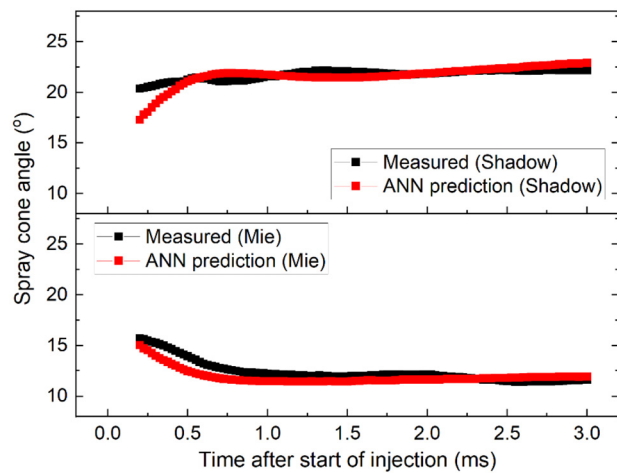


FIG. 14. Validation of spray cone angle over time (case 3).

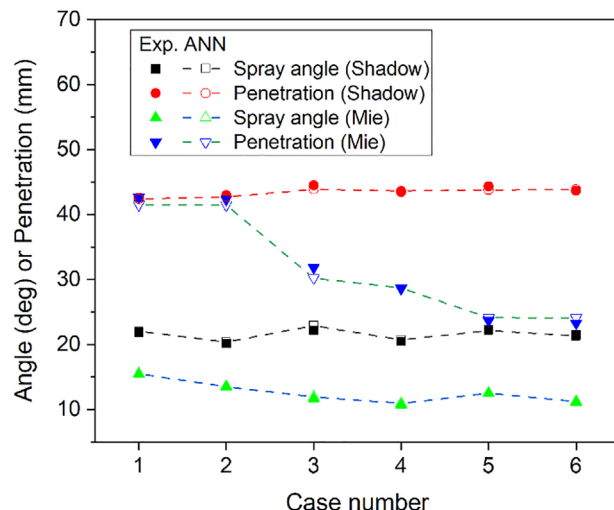


FIG. 15. Comparison of experiment (solid) and ANN model (hollow) at 3 ms.

TABLE III. Prediction error (%) from the ANN model and the measurements at 3 ms.

	Shadow angle	Shadow length	Mie angle	Mie length
Case 1	0.78	-0.44	0.21	-2.69
Case 2	0.93	-0.63	-0.64	-2.00
Case 3	3.32	-1.36	2.42	-4.98
Case 4	1.14	0.40	2.38	0.40
Case 5	-0.68	-1.23	0.19	2.01
Case 6	-0.50	0.36	0.92	3.65

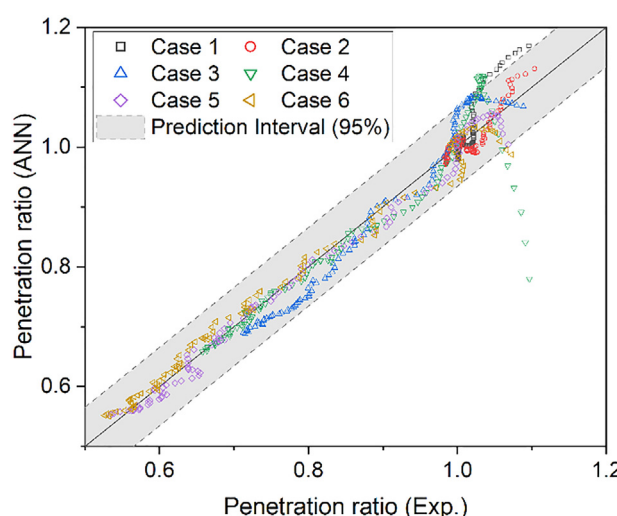


FIG 16. Parity plot comparing the measured and modeled PR.

TABLE IV. Assessment comparison of different ANN layer functions and neurons (N ... Neurons; L1 ... Layer1; L2 ... Layer2; L3 ... Layer3; and P ... PureLn; T ... Tansig; L ... Logsig; θ ... Spray angle; L ... Spray length; S ... Shadowgraphy; and M ... Mie Scattering experiments).

Model trials	Network architecture			MSE				MAPE				R^2			
	L1 N1	L2 N2	L3 N3	θ_S	L_S	θ_M	L_M	θ_S	L_S	θ_M	L_M	θ_S	L_S	θ_M	L_M
1	L10	T4	...	5.07	141	0.34	110	9.62	4.2	1.7	7.8	0.99	0.91	0.97	0.91
2	T10	P4	...	8.1	582	58	899	25.9	1.6	8.6	96.3	0.94	3.5	0.85	10.6
3	P10	T4	...	0.59	1.55	2.35	8.93	3.34	4.22	11.7	10.4	1.00	1.0	0.99	0.99
4	P12	T4	...	0.95	1.66	2.47	9.52	4.23	4.44	11.9	10.6	1.00	1.0	0.99	0.99
5	P14	T4	...	0.69	1.59	1.98	10.1	3.58	4.32	10.7	10.8	1.00	1.0	0.99	0.99
6	P8	T4	...	0.68	1.41	1.68	10.1	3.56	4.01	9.90	10.8	1.00	1.0	0.99	0.99
7	P10	T10	P4	44.7	84.0	39.6	163	30.1	33.7	51.0	47.9	0.81	0.86	0.89	0.30
8	P8	T8	P4	1.61	1.94	28.6	13.0	4.60	5.43	41.5	14.5	1.00	1.00	0.91	0.98
9	P7	T7	P4	2.62	5.12	0.71	5.25	6.34	7.48	5.60	7.89	0.99	0.99	0.99	0.99
10	P6	T6	P4	0.91	0.74	3.01	5.63	3.31	3.00	13.5	7.93	1.00	1.0	0.98	0.99
11	P4	T4	P4	19.5	3.42	2.47	3.62	19.9	5.67	10.9	6.04	0.94	1.0	0.98	0.99
12	P8	T6	P4	5.34	20.8	1.82	10.1	9.71	16.2	9.68	10.0	0.99	0.97	0.99	0.98

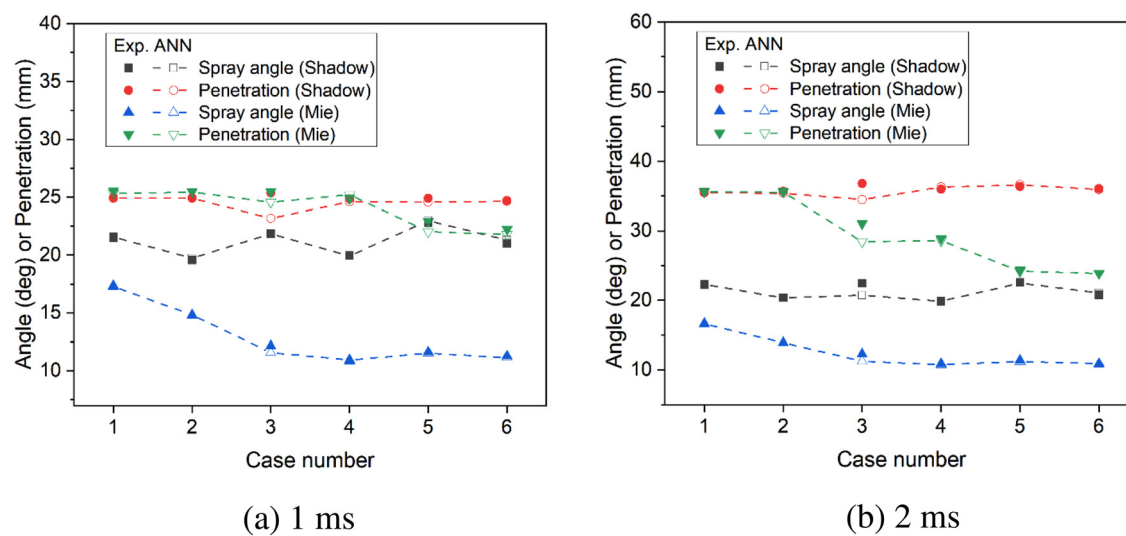


FIG 17. Comparison of experiment (solid) and ANN model (hollow).

shape^{1,41,42}) and wider ranges of injection and chamber conditions. Overall, the study demonstrates the effectiveness of the simple ANN model in predicting spray characteristics and its potential for practical applications in the design and optimization of combustion devices. A more complex ANN model will be part of future work.

ACKNOWLEDGMENTS

The authors acknowledge the Science and Engineering Research Board, India, for awarding the SIRE Fellowship (No. SIR/2022/000042) to conduct this collaborative research. This project also received funding by dtec.bw—Digitalization and Technology Research Center of the Bundeswehr—under the project MaST—Macro-/Micro-simulation of Phase Separation Phenomena in the Transcritical

Regime, which is gratefully acknowledged. The authors thank the group Professur für Fluidsystemtechnik (FST, Professor Michael Wensing), Friedrich-Alexander-Universität Erlangen-Nürnberg (FAU), for support to the experiments. The authors acknowledge financial support by Universität der Bundeswehr München.

AUTHOR DECLARATIONS

Conflict of Interest

The authors have no conflicts to disclose.

Author Contributions

Thangaraja Jeyaseelan: Data curation (equal); Software (lead); Writing – original draft (lead). **Min Son:** Investigation (equal);

Methodology (equal); Validation (equal); Writing – original draft (equal). **Tobias Sander:** Data curation (equal); Formal analysis (equal); Investigation (equal). **Lars Zigan:** Project administration (lead); Supervision (lead); Visualization (equal); Writing – review & editing (equal).

DATA AVAILABILITY

The data that support the findings of this study are available from the corresponding author upon reasonable request.

NOMENCLATURE

I_p	prediction interval of smoothed data
l_{shadow}	spray penetration lengths measured by shadowgraphy
l_{Mie}	spray penetration lengths measured by Mie scattering measurement
m	number of times after start of injection
n	number of injection shots
P_c	chamber pressure
P_{inj}	injection pressure
$P_{r,c}$	reduced chamber pressure
R^2	coefficient of determination
t	time after start of injection
T_c	chamber temperature
T_{inj}	injection temperature
T_{n-1}	Student's t-distribution with $n - 1$ degrees of freedom
$T_{r,c}$	reduced chamber temperature
u	uncertainty of measured point data
U	uncertainty of smoothed data
\bar{U}	mean uncertainty for the smoothed spray angles
ν_{inj}	fuel kinematic viscosity at injection
ε	error of smoothed data
ΔP	injection pressure drop
θ	measured spray angle
$\bar{\theta}$	ensemble-averaged spray angle
ρ_{inj}	fuel density at injection
σ	standard deviation
ANN	artificial neural network
CFD	computational fluid dynamics
GDI	gasoline direct injection
LM	Levenberg–Marquardt
MAPE	mean absolute percentage error
ML	machine learning
MSE	mean square error
PR	penetration ratio
SMD	Sauter mean diameter

APPENDIX: AN OVERVIEW OF THE DEVELOPED ANN MODEL

The following table provides an overview of the ANN model architecture that was trained to predict the spray characteristics of cyclopentane. Initially, the model was attempted with two layers and various combinations of transfer functions, but the resulting errors varied significantly. Consequently, a three-layer network

TABLE V. Prediction error (%) from the ANN model and the measurements at 1 ms.

	Shadow angle	Shadow length	Mie angle	Mie length
Case 1	0.13	0.60	0.03	-0.87
Case 2	1.18	0.51	-0.05	-2.19
Case 3	0.75	-1.65	-6.02	3.39
Case 4	0.59	0.00	-0.08	2.80
Case 5	1.05	1.04	-2.08	-0.25
Case 6	1.03	-0.52	-0.31	-0.83

TABLE VI. Prediction error (%) from the ANN model and the measurements at 2 ms.

	Shadow angle	Shadow length	Mie angle	mie length
Case 1	0.46	-0.03	0.05	0.88
Case 2	-0.64	0.01	0.07	1.38
Case 3	0.12	-0.55	-4.40	-5.00
Case 4	0.28	-0.42	-0.91	-2.23
Case 5	-0.25	-0.48	0.34	1.91
Case 6	0.56	-0.75	0.25	3.53

configuration with seven neurons and a combination of the linear (Purelin) and hyperbolic tangent sigmoid (Tansig) transfer functions produced better results.

REFERENCES

- ¹H. Ulrich, B. Lehnert, D. Guénot, K. Svendsen, O. Lundh, M. Wensing, E. Berrocal, and L. Zigan, "Effects of liquid properties on atomization and spray characteristics studied by planar two-photon fluorescence," *Phys. Fluids* **34**(8), 083305 (2022).
- ²H. Liu, H. Wu, D. Yang, J. Chen, and J. Wang, "A study of the temperature effect on the spray characteristics in the cone-jet mode of electrohydrodynamic atomization (EHDA) with viscous liquids," *Phys. Fluids* **35**(4), 043338 (2023).
- ³F. Li and Q. Lin, "Radial development of pentanol–biodiesel fuel spray in a high-pressure common-rail system," *Phys. Fluids* **33**(9), 95115 (2021).
- ⁴J. Tian, Y. Liu, F. Li, K. Han, W. Zhou, Q. Lin, and K. Meng, "Experimental study on spray characteristics of octanol biodiesel and modification of spray tip penetration model," *Phys. Fluids* **33**(9), 91902 (2021).
- ⁵F. Kafrawi, K. H. Lee, C. Zhang, and S. Bari, "Spray analysis of palm-based biodiesel to correlate performance and combustion analysis of a compression ignition engine," *Fuel* **319**, 123822 (2022).
- ⁶T. Xuan, Z. Sun, A. I. EL-Seesy, Y. Mi, W. Zhong, Z. He, Q. Wang, J. Sun, H. M. El-Batsh, and J. Cao, "An optical study on spray and combustion characteristics of ternary hydrogenated catalytic biodiesel/methanol/n-octanol blends; Part? Liquid length and in-flame soot," *Energy* **227**, 120543 (2021).
- ⁷H. Zhao, *Laser Diagnostics and Optical Measurement Techniques in Internal Combustion Engines* (SAE International, 2012).
- ⁸A. H. Lefebvre and V. G. McDonell, *Atomization and Sprays* (CRC Press, 2017).
- ⁹F. Duronio, A. De Vita, L. Allocata, and M. Anatone, "Gasoline direct injection engines - A review of latest technologies and trends. Part 1: Spray breakup process," *Fuel* **265**, 116948 (2020).
- ¹⁰M. Fathi, S. Hickel, and D. Roekaerts, "Large eddy simulations of reacting and non-reacting transcritical fuel sprays using multiphase thermodynamics," *Phys. Fluids* **34**(8), 085131 (2022).
- ¹¹J. Wang, Z. Wang, X. Hui, M. Han, C. Liu, and W. Tao, "The effects of fuel distribution on exit temperature distribution in a centrally staged combustor," *Phys. Fluids* **35**(6), 065136 (2023).

- ¹²M.-R. Pendar, S. Cândido, and J. C. Páscoa, "Optimization of painting efficiency applying unique techniques of high-voltage conductors and nitrotherm spray: Developing deep learning models using computational fluid dynamics dataset," *Phys. Fluids* **35**(7), 075119 (2023).
- ¹³S. Haykin, *Neural Networks and Learning Machines*, 3rd ed. (Pearson Education India, 2009).
- ¹⁴H. Taghavifar, S. Khalilarya, and S. Jafarmadar, "Diesel engine spray characteristics prediction with hybridized artificial neural network optimized by genetic algorithm," *Energy* **71**, 656–664 (2014).
- ¹⁵J. Hwang, P. Lee, S. Mun, I. K. Karathanassis, P. Koukouvinis, L. M. Pickett *et al.*, "Machine-learning enabled prediction of 3D spray under engine combustion network spray G conditions," *Fuel* **293**, 120444 (2021).
- ¹⁶J. Hwang, P. Lee, S. Mun, I. K. Karathanassis, P. Koukouvinis, F. Tagliante *et al.*, "A new pathway for prediction of gasoline sprays using machine-learning algorithms," SAE Technical Paper (2022-01-0492) (2022).
- ¹⁷M. Wensing, T. Vogel, and G. Götz, "Transition of diesel spray to a supercritical state under engine conditions," *Int. J. Engine Res.* **17**(1), 108–119 (2016).
- ¹⁸S. Lind, U. Retzer, S. Will, and L. Zigan, "Investigation of mixture formation in a diesel spray by tracer-based laser-induced fluorescence using 1-methyl-naphthalene," *Proc. Combust. Inst.* **36**(3), 4497–4504 (2017).
- ¹⁹W. Fu, L. Song, T. Liu, and Q. Lin, "Experimental study of spray characteristics of biodiesel blending with diethyl carbonate in a common rail injection system," *Proc. Inst. Mech. Eng. Part D* **233**(2), 249–262 (2019).
- ²⁰J. Kostas, D. Honnery, and J. Soria, "Time resolved measurements of the initial stages of fuel spray penetration," *Fuel* **88**(11), 2225–2237 (2009).
- ²¹H. Hiroyasu and M. Arai, "Structures of fuel sprays in diesel engines," *SAE Trans.* **99**, 1050–1061 (1990).
- ²²C. E. Ejim, B. A. Fleck, and A. Amirfazli, "Analytical study for atomization of biodiesels and their blends in a typical injector: Surface tension and viscosity effects," *Fuel* **86**(10), 1534–1544 (2007).
- ²³Y. Liu, J. Tang, Z. Song, F. Li, W. Zhou, and Q. Lin, "Spray characteristics of diesel, biodiesel, polyoxymethylene dimethyl ethers blends and prediction of spray tip penetration using artificial neural network," *Phys. Fluids* **34**(1), 015117 (2022).
- ²⁴H. Wu, Z. Zhang, F. Zhang, and W. L. Roberts, "Time-resolved low-pressure air-assisted spray performance and unsteadiness evaluation," *Phys. Fluids* **35**(4), 043335 (2023).
- ²⁵C. Traxinger, M. Pfitzner, S. Baab, G. Lamanna, and B. Weigand, "Experimental and numerical investigation of phase separation due to multicomponent mixing at high-pressure conditions," *Phys. Rev. Fluids* **4**(7), 74303 (2019).
- ²⁶B. T. Austin and K. Sumathy, "Transcritical carbon dioxide heat pump systems: A review," *Renew. Sustainable Energy Rev.* **15**(8), 4013–4029 (2011).
- ²⁷S. Riess, L. Weiss, A. Peter, J. Rezaei, and M. Wensing, "Air entrainment and mixture distribution in Diesel sprays investigated by optical measurement techniques," *Int. J. Engine Res.* **19**(1), 120–133 (2018).
- ²⁸T. Vogel, M. Lutz, M. Wensing, and A. Leipertz, in 23rd Annual Conference on Liquid Atomization and Spray Systems (2010).
- ²⁹A. Montanaro, M. Migliaccio, L. Allocca, V. Fraioli, S.-Y. Lee, A. Zhang, and J. Naber, "Schlieren and Mie scattering visualization for single-hole diesel injector under vaporizing conditions with numerical validation" (2014).
- ³⁰I. H. Bell, J. Wronski, S. Quoilin, and V. Lemort, "Pure and pseudo-pure fluid thermophysical property evaluation and the open-source thermophysical property library CoolProp," *Ind. Eng. Chem. Res.* **53**(6), 2498–2508 (2014).
- ³¹Joint Committee for Guides in Metrology, "Evaluation of measurement data—Guide to the expression of uncertainty in measurement," *International Organization for Standardization, Geneva* (ISO, 2008), Vol. 50, p. 134.
- ³²S. Rajkumar, A. Das, and J. Thangaraja, "Integration of artificial neural network, multi-objective genetic algorithm and phenomenological combustion modelling for effective operation of biodiesel blends in an automotive engine," *Energy* **239**, 121889 (2022).
- ³³S. Geisser, *Predictive Inference* (Chapman and Hall/CRC, 2017).
- ³⁴W. E. Anderson and V. Yang, *Liquid Rocket Engine Combustion Instability* (American Institute of Aeronautics and Astronautics, 1995).
- ³⁵W. Armbruster, J. S. Hardi, D. Suslov, and M. Oschwald, "Injector-driven flame dynamics in a high-pressure multi-element oxygen-hydrogen rocket thrust chamber," *J. Propuls. Power* **35**(3), 632–644 (2019).
- ³⁶B. Ghobadian, H. Rahimi, A. M. Nikbakht, G. Najafi, and T. F. Yusaf, "Diesel engine performance and exhaust emission analysis using waste cooking biodiesel fuel with an artificial neural network," *Renew. Energy* **34**(4), 976–982 (2009).
- ³⁷N. Motamedifar and A. Shirneshan, "An experimental study of emission characteristics from cylindrical furnace: Effects of using diesel-ethanol-biodiesel blends and air swirl," *Fuel* **221**, 233–239 (2018).
- ³⁸J. Thangaraja, L. Zigan, and S. Rajkumar, "A machine learning framework for evaluating the biodiesel properties for accurate modeling of spray and combustion processes," *Fuel* **334**, 126573 (2023).
- ³⁹Y. Xiao, L. M. Yang, Y. J. Du, Y. X. Song, and C. Shu, "Radial basis function-differential quadrature-based physics-informed neural network for steady incompressible flows," *Phys. Fluids* **35**(7), 073607 (2023).
- ⁴⁰X. Li, Y. Liu, and Z. Liu, "Physics-informed neural network based on a new adaptive gradient descent algorithm for solving partial differential equations of flow problems," *Phys. Fluids* **35**(6), 063608 (2023).
- ⁴¹M. Storch, M. Koegl, M. Altenhoff, S. Will, and L. Zigan, "Investigation of soot formation of spark-ignited ethanol-blended gasoline sprays with single-and multi-component base fuels," *Appl. Energy* **181**, 278–287 (2016).
- ⁴²L. Zigan, I. Schmitz, A. Flügel, M. Wensing, and A. Leipertz, "Structure of evaporating single-and multicomponent fuel sprays for 2nd generation gasoline direct injection," *Fuel* **90**(1), 348–363 (2011).